Communication-Free Adaptive Protection of Microgrids Using Support Vector Machines

Rakhi[1], Nishant Patnayak[2]
1,2Department of Electrical Engineering, RSR Rungta College of Engineering and Technology, Bhilai, India.
1rakhisrit@gmail.com, 2nishanthpatnaik_eee@cbit.ac.in

Abstract
Inverter-based generation changes how distribution networks must be protected. When a microgrid separates from the main grid, fault current falls to little more than the inverters' limited output, and overcurrent relays tuned for grid-connected operation lose sensitivity or respond too slowly. This paper presents an adaptive protection scheme that identifies the operating mode and detects faults from measurements at a single relay point. A three-phase 33/11 kV microgrid with battery and PV inverter sources, switched loads, and ten fault types was built in Simulink. Two support vector machines, one for mode and one for faults, use one-cycle phasor, sequence-component and superimposed-quantity features. The detected mode selects the relay's setting group, and the fault detector trips after two consecutive positive decisions. The scheme was compared with a conventional relay using standard-inverse and instantaneous overcurrent elements on the same cases. Across 39 fault cases, the adaptive relay detected every fault in about 12 ms on average in both modes, with no false trips on 21 load-switching and motor-starting events. The conventional relay cleared no islanded fault within the simulated window and detected half of the grid-connected faults. The results are based on a simplified source model and a small simulated test set, and hardware-in-the-loop validation remains future work.

Keywords—adaptive protection, microgrid, islanded operation, inverter-based resources, support vector machine, fault detection

I. INTRODUCTION

The rapid adoption of distributed energy resources (DERs) is changing the way power is delivered at the distribution level. Solar PV plants, battery storage systems and other inverter-interfaced sources are increasingly grouped into microgrids, which can serve local loads while connected to the main grid or operate independently as an island when the grid is lost [1], [2]. This ability improves reliability and allows higher penetration of renewable energy, but it also creates a serious protection problem.

Distribution networks have traditionally been protected by overcurrent relays set on the assumption that a fault is fed from a single, strong upstream source. In a grid-connected microgrid this assumption holds reasonably well, and fault currents are many times the load current. When the microgrid islands, the situation changes sharply. The grid contribution disappears, and the remaining sources are mostly power electronic converters whose output current is deliberately limited to roughly 1.1 to 1.5 times rated current to protect their semiconductor switches [3], [4]. Fault current in the islanded mode can therefore be a small fraction of its grid-connected value, and in some cases it is hardly distinguishable from the current drawn by a heavy load or a motor start.

This creates a conflict that fixed relay settings cannot resolve. A pickup setting chosen for the grid-connected mode may be too high to see an islanded fault at all. A setting chosen for the islanded mode would be too sensitive in the grid-connected mode and could trip on normal disturbances, losing coordination with other devices. Because inverse-time curves also operate slowly at low current multiples, a fault that is detected in the islanded mode may be cleared far too late to protect equipment or maintain voltage quality [5].

Adaptive protection has been proposed as a way to address this problem. In such schemes the relay settings are changed according to the network configuration, typically by switching between predefined setting groups when the operating mode changes [6], [7]. Many of these approaches rely on communication links to report breaker status, which adds cost and a possible point of failure. In parallel, machine learning methods, including support vector machines and neural networks, have been applied to fault detection and classification in microgrids using features drawn from voltage and current measurements [8], [9]. However, many of these studies treat fault detection and operating-mode identification as separate problems, or evaluate their classifiers on extracted data rather than in a complete time-domain simulation where the relay acts on live waveforms.

This paper addresses that gap. It presents a protection scheme that identifies the operating mode and detects faults from local measurements at a single relay point, without a communication link. The detected mode selects the relay's setting group, and a fault detector trained on one-cycle phasor and sequence-component features issues the trip. The contributions of this work are as follows:

- A three-phase Simulink model of a 33/11 kV microgrid with battery and PV inverter sources, in which islanding, ten fault types, load switching and motor starting can be simulated.
- A mode-aware adaptive relay using support vector machines, implemented inside the simulation so that it operates on live sampled signals.
- A comparison with a conventional relay with standard-inverse and instantaneous overcurrent elements, using the same cases, in terms of detection rate, detection time and false trips.

The remainder of the paper is organised as follows. Section II reviews related work. Section III describes the system model and the simulated scenarios. Section IV presents the proposed method. Section V reports and discusses the results, and

ISSN: **3107-6513**

Section VI states the limitations and directions for future work. Section VII concludes the paper.

II. LITERATURE REVIEW

A. Protection challenges in converter-dominated microgrids

Distribution protection was designed around one-way power flow, with time-coordinated overcurrent relays as the standard tool [1]. Distributed generation and microgrids undermine that assumption. A review of medium-voltage microgrids with converter-interfaced sources found that current-magnitude relays fail to operate when the microgrid is islanded. In grid-connected operation they operate late or not at all for some fault locations, and they can also suffer relay blinding and sympathetic tripping [2]. A broader review makes the same point: most DG units connect through DC-to-AC converters that limit fault current, so a suitable scheme must work in both operating modes [3]. The converter behaviour is quantified in industry material: inverter controls limit output current to a value near rated, within about two cycles of a fault. In one PSCAD example, the current stayed nearly balanced and below 110% of its pre-fault value [4]. This is the root of the problem addressed in this paper, because it leaves little current for a fixed-setting overcurrent relay to see. Microgrid Protection: Technical challenges and existing techniques +3

B. Adaptive protection

Adaptive protection addresses this by letting devices change their settings when the system state changes [5]. In practice, multifunction relays hold a small number of selectable setting groups (typically four to eight), each calculated for a different operating configuration [6]. In setting-group schemes, the active group is selected from the prevailing conditions, including the microgrid's mode of operation [7]. Most of the schemes reviewed rely on communication to coordinate the relays, which in turn demands high availability and latency of only a few milliseconds [5]. This dependence has motivated a recent survey arguing for communication-free adaptive methods [8]. The scheme in this paper follows that direction: the mode is inferred locally from the relay's own measurements. Review of the State-of-the-Art on Adaptive Protection for Microgrids based on Communications +4

C. Machine learning for microgrid fault detection

Machine learning has been widely applied to the detection and classification of microgrid faults. One scheme combined wavelet-packet features with an SVM tuned by particle swarm optimisation and ran it on a real-time digital simulator, with islanded and non-islanded cases [9]. Another used SVMs on voltage and current features and covered operation with and without grid interconnection, including fault location and resistance variation and, for non-fault cases, load changes [10]. A combination of an adaptive neuro-fuzzy system and an SVM was tested on a 12-bus AC microgrid in both islanded and grid-connected modes, targeting low fault current and high-impedance faults [11]. A two-level SVM adaptive scheme reported identification of faulted lines and fault types within a cycle in both modes [12]. For islanded AC microgrids with meshed topology, an SVM-based method was proposed because legacy overcurrent schemes are ineffective there [13]. Work on DC microgrids has also treated mode identification as a first stage, followed by fault detection, classification and section identification [14]. Energy Reports (Nov 2022) +5

D. Research gap and contribution

Two observations follow from this body of work. First, learning-based detectors are usually evaluated on datasets extracted from simulation. Their classifiers are then rarely embedded in a time-domain model where a relay acts on live sampled signals and its trip time is measured. Second, comparisons with a conventional fixed-setting relay under identical cases, including non-fault disturbances such as motor starting, are less common.

This paper does not claim that mode-aware learning-based protection is new, since mode identification followed by fault detection has been reported before [12], [14]. Its contribution is narrower and practical: a single-point, communication-free relay with a mode classifier and a fault detector, implemented inside a three-phase Simulink microgrid so that it runs on live signals, and compared against a static inverse-time and instantaneous relay on the same islanding, fault, load-switching and motor-start cases.

III. SYSTEM MODEL

A. Test microgrid

The study system is a radial 11 kV, 50 Hz microgrid modelled in Simulink with Simscape Electrical, shown in Fig. 1. A 33 kV utility source with a short-circuit level of 200 MVA and an X/R ratio of 10 supplies the network through a 33/11 kV, 10 MVA transformer. A point-of-common-coupling (PCC) breaker connects the transformer to the microgrid. The breaker is closed in grid-connected cases and opens at 0.20 s in islanded cases.

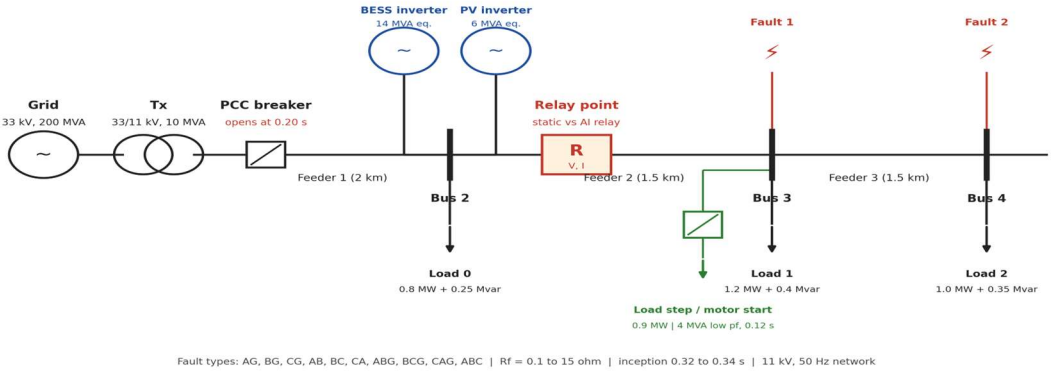

ISSN: **3107-6513**

Fig. 1. Single-line diagram of the simulated 11 kV, 50 Hz microgrid, showing the utility source, the PCC breaker, the BESS and PV inverter sources, the three feeders, the relay point and the fault locations.

Downstream of the PCC, three feeder sections of 2 km, 1.5 km and 1.5 km are modelled as three-phase PI sections and join Buses 2, 3 and 4. Two inverter-based sources, a battery energy storage system (BESS) and a PV unit, are connected at Bus 2. Three base loads are connected at Buses 2, 3 and 4, with a nominal total of 3.0 MW and 1.0 Mvar. The protection relay is placed between Bus 2 and Bus 3, so it covers Feeder 2 and everything downstream of it. Its signals are three-phase voltage and current. Parameters are listed in Table I.

TABLE I. NETWORK PARAMETERS

Element	Parameters
Utility source	33 kV, 50 Hz, 200 MVA short-circuit level, X/R = 10
Transformer	33/11 kV, 10 MVA, Yg–Yg, R = 0.002 pu, L = 0.05 pu
Feeders 1, 2, 3	2 km, 1.5 km, 1.5 km; R1/R0 = 0.25/0.7 Ω/km; L1/L0 = 1.2/4 mH/km; C1/C0 = 12/8 nF/km
BESS inverter source	11.33 kV (1.03 pu), 14 MVA short-circuit equivalent, X/R = 5
PV inverter source	11.33 kV (1.03 pu), 6 MVA short-circuit equivalent, X/R = 5
Load 0 (Bus 2)	0.8 MW + 0.25 Mvar
Load 1 (Bus 3)	1.2 MW + 0.40 Mvar
Load 2 (Bus 4)	1.0 MW + 0.35 Mvar
Base values	11 kV line voltage, 200 A rms current (1 pu)

B. Inverter-based sources

The inverter sources are represented as three-phase voltage sources behind a source impedance set from the short-circuit-level parameter, rather than as detailed inverter models with current control. This keeps the islanded fault level low and bounded: with the grid disconnected, the two sources together can supply a bolted-fault current of about 20 MVA / ($\sqrt{3}$ × 11 kV) ≈ 1.05 kA at their terminals, much less than the grid-connected fault level. It does not reproduce the fast current-limiting loop of a real inverter, so the model captures the reduction in fault level on islanding but not the converter's control dynamics. This limitation is discussed in Section VI.

C. Operating scenarios

Each simulated case is 0.55 s long and combines an operating mode with one event. Table II lists the variables.

TABLE II. SCENARIO VARIABLES

Variable	Values
Operating mode	Grid-connected, or islanded (PCC opens at 0.20 s)
Event type	Fault (about 60% of cases), load switching (20%), motor starting (20%)
Fault type	AG, BG, CG, AB, BC, CA, ABG, BCG, CAG, ABC
Fault location	Bus 3 or Bus 4
Fault resistance	0.1, 0.5, 2, 5, 10, 15 Ω (ground resistance 0.01 Ω)
Event inception	Random, between 0.32 and 0.34 s
Load level	70% to 115% of nominal base loads
Load switching	0.9 MW + 0.44 Mvar added at Bus 3 and kept connected
Motor starting	1.2 MW + 3.8 Mvar (about 4 MVA, low power factor) connected for 0.12 s

Load switching and motor starting are non-fault disturbances, so a correct relay must not trip on them. Faults persist until the end of the simulation.

D. Measurement chain

The relay's voltages and currents are scaled to per unit and sampled at 3200 Hz (64 samples per cycle). Gaussian noise of variance 10^{-5} pu^2 is added to each channel. The model runs with a fixed 62.5 µs solver step. Relay logic is armed after 0.15 s, so the start-up transient from zero initial conditions does not affect trip decisions.

IV. PROPOSED METHOD

A. Overview

The proposed relay uses only local three-phase voltage and current at one relay point. It has three stages (Fig. 2): feature extraction from sliding one-cycle windows, two support vector machines (SVMs) that identify the operating mode and detect a fault, and a trip rule that also selects the setting group of a backup overcurrent element from the detected mode. A third SVM, used offline, classifies the fault type. No communication link or breaker-status signal is used. The mode is inferred from the relay's own measurements.

[Fig. 2 to be inserted here: sampled voltage and current → windowed feature extraction → mode SVM and fault SVM → trip logic, with the setting-group selector feeding the backup 51 element.]

Fig. 2. Block diagram of the proposed adaptive relay.
Fig. 3.

B. *Feature extraction*

The per-unit signals are sampled at 3200 Hz (N = 64 samples per cycle). A decision is made every 16 samples (5 ms) from a buffer of 144 samples. In each window, peak-amplitude phasors of order h are computed by a discrete Fourier transform,

$$X_h = (2/N)\,\Sigma\, x[n] \cdot \exp(-j2\pi \cdot h \cdot f_0 \cdot n / f_s),$$

for voltages and currents (h = 1), and for the fifth harmonic (h = 5) in the mode features. Sequence components follow from the symmetrical-component transform. Subscripts 0, 1 and 2 denote zero, positive and negative sequence. The phasors are also computed for the window one cycle earlier, so that superimposed quantities, which respond to a change and not to a steady load level, can be formed.

The fault detector uses 12 features: the maximum phase current; the largest change in a phase current compared with one cycle earlier; the minimum phase voltage; the largest change in a phase voltage; the magnitudes of I_2, I_0, V_2 and V_0; the change in the angle between I_1 and V_1; the changes in $|I_1|$ and $|V_1|$; and the ratio of the maximum phase current to its value one cycle earlier. The detected mode is added as a thirteenth input.

The mode classifier uses seven features: the frequency deviation (from the phase advance of the phase-A voltage between two windows 16 samples apart); the fifth-harmonic ratios of voltage and current; the deviation of $|V_1|$ from 1 pu; the ratio V_2/V_1; and $|I_1|$ with its angle relative to V_1. These are averaged over up to the last five steady-state windows. A window is treated as steady when the current and voltage changes are small (below 0.1 and 0.02 pu), the minimum voltage is above 0.75 pu, and the maximum current is below 1.4 pu. Mode memory is therefore not updated during a fault or large disturbance.

C. *Classifiers and training*

All three classifiers are SVMs with a radial-basis kernel, standardised inputs, a box constraint of 10 and an automatically selected kernel scale. The mode SVM has two classes, grid-connected and islanded. The fault SVM separates "fault" from "no fault". The offline fault-type classifier is a multi-class SVM with ten classes. Its inputs are the phase current changes normalised by their maximum, the three phase-voltage magnitudes, I_0 and I_2 normalised by the maximum current, and V_0 and V_2.

Training data come from 200 random Simulink cases with the scenario variables in Table II, split 70/30 by event so that windows of the same event never appear in both sets. For the fault SVM, windows before the event are labelled "no fault". After inception, windows that end at least 24 samples later are labelled "fault" for fault events and "no fault" for load switching and motor starting. The transition windows in between are excluded. Up to 4,000 windows are used for training. In testing, the fault SVM receives the mode predicted by the mode SVM, not the true mode. The trained SVM parameters are exported into the relay block, after a numerical check that the exported function reproduces the toolbox prediction.

D. *Adaptive relay logic*

The relay evaluates the fault SVM every 5 ms. It trips when two consecutive decisions are positive, which reduces the effect of isolated misclassified windows. Tripping is latched. The mode estimate updates only during steady-state windows and is frozen after a trip. Mode selects the setting group of a backup inverse-time overcurrent element (Table III), which runs alongside the SVM and trips if its integrator reaches one. It uses the IEC standard-inverse curve,

$$t = TMS \cdot 0.14 / (M^{0.02} - 1),\ M = I / I_{pickup}.$$

TABLE III. RELAY SETTINGS

Relay	Element	Settings
Static	51 (standard inverse)	pickup 1.25 pu, TMS 0.10
Static	50 (instantaneous)	6.0 pu (one-cycle rms)
AI adaptive, grid-connected group	backup 51	pickup 1.25 pu, TMS 0.10
AI adaptive, islanded group	backup 51	pickup 1.05 pu, TMS 0.05
AI adaptive	SVM trip rule	two consecutive positive 5 ms decisions

Algorithm steps, per 5 ms decision:

- Update the current and voltage buffers and compute the windowed features.
- If the window is steady, update the mode memory and re-classify the operating mode.
- Evaluate the fault SVM with the 12 features and the mode.
- Trip if the last two decisions are positive, or if the backup element has timed out.

E. *Static relay and evaluation*

The static baseline uses a standard-inverse 51 element and a 50 element with the fixed settings in Table III. Both relays are armed after 0.15 s. The relays are compared on the same fresh random test cases using the detection rate for fault cases, the detection time from fault inception to trip, and the number of false trips on load switching and motor starting.

V. RESULTS AND DISCUSSION

A. *Test setup and metrics*

After training, both relays were run inside the Simulink model on 60 new random cases, generated independently of the training data with the scenario variables in Table II. Of these, 39 were faults (16 grid-connected, 23 islanded) and 21 were load-switching or motor-starting events. Three metrics are reported: the fault detection rate (the share of faults that produced a trip), the detection time (from fault inception to trip, averaged over detected faults), and the number of false trips on non-fault events. Each case ran for 0.55 s, so a fault was observed for about 0.21 to 0.23 s after inception. A fault that did not trip within this window counts as not detected. The detection time of the AI relay moves in steps of about 5 ms, because decisions are made every 16 samples.

B. *Classifier performance*

On held-out events, the mode classifier, the fault detector (window level, AUC = 1.00) and the fault-type classifier all scored 100%. These figures show that the three tasks are separable in the simulated data. They should not be read as a general accuracy claim, for two reasons. The training and test cases come from the same simulator with small sensor noise, and the test split is small (about 60 held-out events). Papers on

similar SVM schemes also report very high accuracy, for example above 99.99% in one study [10] and fault identification within one cycle in both modes in another [12], but those results are for different networks, so I do not compare the numbers directly.

C. *Detection performance*

Table IV and Fig. 3 summarise the comparison.

TABLE IV. STATIC VERSUS AI ADAPTIVE RELAY ON THE TEST CASES

Mode	Fault cases	Static relay detected	Static mean time	AI relay detected	AI mean time
Grid-connected	16	8 (50%)	8.9 ms	16 (100%)	12.7 ms
Islanded	23	0 (0%)	no trip in window	23 (100%)	11.3 ms
All faults	39	8 (20.5%)	8.9 ms	39 (100%)	11.9 ms
Non-fault events	21	0 false trips	N/A	0 false trips	N/A

[Fig. 3 to be inserted here: comparison of detection rate and mean detection time for the static and AI relays, grid-connected, islanded and all faults.]

Fig. 4. Detection rate and mean detection time of the static and adaptive relays.

The AI relay detected all 39 faults, in about 12 ms on average, with similar times in both modes. The static relay detected only half of the grid-connected faults, and it detected none of the islanded ones within the simulated window.

The static relay's detections came from its instantaneous element, which acts at about one cycle of rms measurement when the current exceeds 6 pu. In those cases it was slightly faster than the AI relay, and that should be stated plainly. The AI relay's advantage is consistency: it reached a decision on every fault, whatever the fault current level.

D. *Example case*

Fig. 4 shows an islanded phase-A-to-ground fault at Bus 4 with 2 Ω fault resistance, inception at 0.33 s. The PCC current falls to zero at about 0.20 s when the breaker opens. At the relay point, the faulted phase current rises to about 3.5 pu while the others stay near their load values. The static relay's current measurement settles near 3.6 pu, above its 1.25 pu pickup. Its inverse-time integrator rises only slowly, to about 0.3 of its trip threshold by the end of the 0.55 s run, so no trip occurs. Extrapolating the slope suggests a trip about 0.7 s after the fault, which is an estimate and not a simulated result. The AI relay's fault flag rises within a few milliseconds of inception and the trip follows about 8 ms after the fault.

[Fig. 4 to be inserted here: relay-point currents, static relay measurement and inverse-time integrator, and the AI relay fault flag and trip for the example case.]

Fig. 5. Islanded phase-A-to-ground fault at Bus 4 with 2 Ω fault resistance.

E. *Security*

Neither relay tripped on the 21 load-switching and motor-starting cases. For the static relay this is expected, since the 0.12 s motor-start current decays before its integrator can reach the threshold. For the AI relay, it shows that the superimposed and sequence features separate these disturbances from faults in this model. With only 21 non-fault cases, a zero count supports only a modest conclusion: a one-sided 95% bound on the true false-trip rate is about 13%. Similarly, 39 of 39 detections give a lower bound of about 93% on the detection rate. A larger test set is needed for firmer claims.

F. *Discussion*

In this model, the static relay's problem in islanded operation is delay and not blindness. The islanded fault current at the relay (about 3.6 pu in the example) is still above the 1.25 pu pickup, so the 51 element picks up, but the inverse-time curve is slow at that current multiple and the 6 pu instantaneous element is never reached. The inverter sources here are source-impedance equivalents with a fault level well above that of a current-limited inverter, so the model does not show the complete loss of overcurrent sensitivity that real inverters can cause. In a network with tighter inverter limiting, the static relay would perform worse than shown. The result should therefore be read as a conservative demonstration of the static relay's weakness.

Several other points qualify the comparison. The static relay's settings are one reasonable choice, and a lower instantaneous pickup or a definite-time element would change its numbers, although a setting that suits the islanded mode would risk nuisance trips in the grid-connected mode. The AI relay's time is quantised by the 5 ms decision step and includes the window fill time, so 12 ms should not be compared with the sub-cycle times of hardware relays. The relay logic is armed after 0.15 s, and the detected-mode signal in the AI-relay scope switches near 0.045 s, before the breaker opens. This comes from the start-up transient from zero initial conditions and did not affect any trip, but it means that scope does not by itself demonstrate mode tracking. Mode accuracy was assessed on steady windows just before the event.

VI. LIMITATIONS AND FUTURE WORK

This study has several limitations that bound how far its results can be generalised.

Source model. The battery and PV sources are voltage sources behind a source impedance, not inverters with current-control loops. They reproduce the fall in fault level when the microgrid islands, but not the fast current limiting, the positive-sequence-dominated fault current, or the control-dependent angle of a real converter. The islanded fault level here (about 5 pu on a 200 A base) is higher than that of a current-limited inverter, so the static relay's weakness is probably understated. Future work should replace these sources with detailed average-value or switching inverter models, including grid-forming and grid-following control.

Data and test set. The classifiers were trained and tested on cases from one simulated network, with ideal instrument transformers and small Gaussian noise. The 100% accuracies and the 60 test cases therefore support only a modest conclusion. A larger and more varied test set is needed, with other network topologies, load and generation levels, noisier signals, harmonics, CT saturation and measurement errors. Transformer inrush and capacitor switching should be added as non-fault disturbances.

Fault coverage. Fault resistance only reached 15 Ω, and faults were placed only downstream of the relay at two buses. High-impedance faults, evolving faults and faults upstream of the relay were not studied, and the Yg–Yg transformer neglects the phase shift of a delta-star unit.

Real-time claim. The relay runs inside an offline simulation with 5 ms decisions, so the reported times show the algorithm's detection delay, not the performance of a hardware relay. Hardware-in-the-loop testing on a real-time simulator with a digital relay is needed to validate execution time, communication-free operation and numerical robustness.

Protection scope. Only one relay point was considered, and the static baseline used a single reasonable set of settings. Future work should extend the scheme to several relays with coordination and backup, compare against other baselines such as dual-setting or directional relays, and test whether the mode classifier remains reliable during islanding transients and when generation changes.

VII. CONCLUSION

This paper presented a communication-free adaptive protection scheme for a microgrid that switches between grid-connected and islanded operation. The relay works from three-phase voltage and current at a single point. Two support vector machines infer the operating mode and detect faults from one-cycle phasor, sequence-component and superimposed-quantity features. The detected mode selects the setting group of a backup overcurrent element. The scheme was implemented inside a three-phase Simulink model of an 11 kV microgrid with battery and PV sources, and compared with a static relay with standard-inverse and instantaneous elements on the same simulated cases.

On 60 new test cases, the adaptive relay detected all 39 faults, in about 12 ms on average in both operating modes, and gave no false trips on 21 load-switching and motor-starting events. The static relay detected half of the grid-connected faults and none of the islanded faults within the 0.55 s simulation. Where the static relay did trip, through its instantaneous element, it was slightly faster. The practical benefit of the adaptive relay is therefore its consistency across modes and fault levels, not a speed advantage on severe faults.

These results come from a simplified source model, a single simulated network and a small test set, so they show that the approach is feasible and not that it is ready for deployment. Future work should add detailed inverter models, a broader and noisier test set, high-impedance faults and multi-relay coordination, followed by hardware-in-the-loop validation to confirm real-time performance.

REFERENCES

[1] G. Buigues, A. Dyśko, V. Valverde, I. Zamora, E. Fernández, "Microgrid protection: technical challenges and existing techniques," Renewable Energy and Power Quality Journal, doi: 10.24084/repqj11.262.
[2] R. Mohanty, P. Chen, A. T. Le, A. Narula, "Challenges in protection of converter dominated medium-voltage microgrids," Proc. IEEE PES ISGT-Europe, Bucharest, 2019, doi: 10.1109/ISGTEurope.2019.8905739.
[3] Z. Alhadrawi, M. N. Abdullah, H. Mokhlis, "Review of microgrid protection strategies: current status and future prospects," TELKOMNIKA, vol. 20, no. 1, doi: 10.12928/telkomnika.v20i1.19652.
[4] "Microgrid protection systems," PACW, pacw.org/microgrid-protection-systems (web resource, authors not listed).
[5] D. Gutierrez-Rojas, P. H. J. Nardelli, G. Mendes, P. Popovski, "Review of the state-of-the-art on adaptive protection for microgrids based on communications," arXiv:2007.13479, 2020.
[6] "Adaptive protection" conference paper hosted at osti.gov/servlets/purl/1863312 (title and authors to be confirmed from the PDF).
[7] Setting-group adaptive overcurrent protection paper, IIT BHU repository (title and authors to be confirmed from the PDF).
[8] M. Jaffer, A. Ismail, H. M. Khalid, "A need for communication-free adaptive protection strategy in microgrids: an integrated survey," Applied Energy, vol. 390, 2025.
[9] M. Ahmadipour et al., "A novel microgrid fault detection and classification method using maximal overlap discrete wavelet packet transform and an augmented Lagrangian particle swarm optimization-support vector machine," Energy Reports, vol. 8, pp. 4854–4870, 2022, doi: 10.1016/j.egyr.2022.03.174.
[10] P. Venkata, "Data mining model based differential microgrid fault classification using SVM considering voltage and current distortions," J. Operation and Automation in Power Engineering, 2023, doi: 10.22098/joape.2023.10185.1722.
[11] A. Kurmaiah, C. Vaithilingam, "Optimization of fault identification and location using adaptive neuro-fuzzy inference system and support vector machine for an AC microgrid," IEEE Access, vol. 13, pp. 20599–20619, 2025, doi: 10.1109/ACCESS.2025.3534147.
[12] R. Aiswarya, D. S. Nair, T. Rajeev, V. Vinod, "A novel SVM based adaptive scheme for accurate fault identification in microgrid," Electric Power Systems Research, 2023, doi: 10.1016/j.epsr.2023.109439.
[13] "Support vector machine based fault location identification in microgrids using interharmonic injection," Energies, vol. 14, no. 8, 2317, 2021, doi: 10.3390/en14082317 (authors to be added).
[14] S. P. Tiwari et al., "Artificial neural network based algorithm for fault detection in a ring DC microgrid under diverse fault conditions," Distributed Generation & Alternative Energy Journal, vol. 38, no. 1, pp. 23–40.
[15] N. Hatziargyriou, H. Asano, R. Iravani, C. Marnay, "Microgrids," IEEE Power and Energy Magazine, vol. 5, no. 4, pp. 78–94, 2007, doi: 10.1109/MPAE.2007.376583.
[16] N. Baeckeland et al., "Overcurrent limiting in grid-forming inverters: a comprehensive review and discussion," IEEE Transactions on Power Electronics, vol. 39, no. 11, pp. 14493–, Nov. 2024 (end page to be added).
[17] X. Lyu, J. Xie, T. E. McDermott, "Impact of inverter-based resources on grid protection: a review of negative-sequence current generation," Pacific Northwest National Laboratory, Rep. PNNL-36069, 2024.
[18] "Comprehensive review of fault detection and protection strategies for medium-voltage networks supplied by grid-forming inverter sources," Energies, vol. 19, no. 9, art. 2175 (authors to be added; mdpi.com/1996-1073/19/9/2175).
[19] C. Cortes and V. Vapnik, "Support-vector networks," Machine Learning, vol. 20, no. 3, pp. 273–297, 1995, doi: 10.1007/BF00994018.
[20] C. L. Fortescue, "Method of symmetrical co-ordinates applied to the solution of polyphase networks," Trans. AIEE, vol. 37, pt. II, pp. 1027–1140, 1918, doi: 10.1109/T-AIEE.1918.4765570.
[21] IEC 60255-151:2009, "Measuring relays and protection equipment – Part 151: Functional requirements for over/under current protection," 2009.
[22] P. H. A. Barra, V. A. Lacerda, R. A. S. Fernandes, D. V. Coury, "A hardware-in-the-loop testbed for microgrid protection considering non-standard curves," Proc. IPST, 2021.
[23] "Machine learning-based protection and fault identification of 100% inverter-based microgrids" (NSF PAR record 10537954; authors and venue to be added).
[24] "Hardware-in-the-loop validation of optimal adaptive protection for utility networked microgrid applications," Sandia National Laboratories, 2025 (authors to be added).